


Dawid Wajnert  ¹

A field-circuit model of the hybrid magnetic bearing

The paper presents a simulation model of the hybrid magnetic bearing dedicated to simulations of transient state. The proposed field-circuit model is composed of two components. The first part constitutes a set of ordinary differential equations that describes electrical circuits and mechanics. The second part of the simulation model consists of parameters such as magnetic forces, dynamic inductances and velocity-induced voltages obtained from the 3D finite element analysis. The MATLAB/Simulink software was used to implement the simulation model with the required control system. The proposed field-circuit model was validated by comparison of time responses with the prototype of the hybrid magnetic bearing.

1. Introduction

A magnetic bearing (MB) is the electromechanical machine that utilizes magnetic forces to suspend a rotor without mechanical contact. Therefore, MBs are more often fitted in high speed machines due to their contactless operation [1].

An application of permanent magnets in the construction of the magnetic bearing significantly reduces energy consumption. According to the authors [2], a 6-pole radial hybrid magnetic bearing (HMB) uses 86.65% less electricity than a traditional 8-pole active magnetic bearing with the same load capacity. However, permanent magnets can cause saturation of the magnetic circuit and increase magnetic leakage flux. Complicated construction of the HMB requires an interdisciplinary approach to dynamic simulations. Author of the paper [3] proposed the time stepping finite element model (FEM) of the active magnetic bearing that is composed of two components. The first part constitutes ordinary differential equations of electrical circuits and mechanics. Whereas, the second part consists

✉ D. Wajnert, e-mail: d.wajnert@po.opole.pl

¹Opole University of Technology, Department of Electrical Engineering and Mechatronics, Opole, Poland.



of a two-dimensional (2D) electromagnetic FEM of the MB that is solved at every simulation step. The proposed simulation model features good accuracy and allows considering eddy currents and hysteresis losses in the simulation. However, its disadvantage is a 2D solution of the magnetic field that causes significant errors for the studied HMB. On the other hand, the use of the 3D FEM instead of 2D in the time stepping FEM significantly increases simulation time. The similar approach with regard to the electrical gear box was presented in the paper [4].

A different approach is presented in the paper [5], where authors proposed a field-circuit model (FCM) dedicated to dynamic simulations of the electromagnetic actuator. Their model comprises two components, as well. The first part constitutes equations of electrical circuits and mechanics, while the second part consists of parameters calculated from a finite element analysis. In comparison to the time stepping FEM, parameters of the actuator were calculated beforehand and were included in the simulation model as look-up tables. Unfortunately, the authors also used 2D finite element analysis to compute the required parameters. The comparable approach has been adopted by authors of the papers [6–8]. An analogous simulation model of the motor with permanent magnets whose parameters were calculated from the 3D FEM was proposed by the authors [9, 10].

Another approach for the transient state simulation in active magnetic bearings was introduced by authors of the paper [11]. The simulation model includes two components. The first part includes equations of electrical circuits and mechanics, while the second part consists of the magnetic equivalent circuit of the AMB that is solved at every simulation step. Unfortunately, the authors did not present the concordance between the simulation model and the real object.

This paper presents the FCM of the 6-pole radial HMB, whose parameters like the magnetic force, dynamic inductances and velocity-induced voltages were derived from 3D finite element analysis. A set of ordinary differential equations that described circuit part of the HMB were obtained from the Euler-Lagrange formulation. The simulation model with required controllers was prepared in MATLAB/Simulink software. The aim of this paper is to create a dynamic simulation model of the HMB that can be used for analysis of the HMB performance and control strategy testing.

2. Description of the hybrid magnetic bearing

Fig. 1 depicts the considered HMB installed in the housing. It has six salient poles with three permanent magnets N38 and three windings. Permanent magnets are installed in cut spaces of the poles to provide the bias flux. The stator and rotor of the HMB are made of dynamo steel M400-50A in order to reduce eddy currents.

Fig. 2 presents the cross-section of the HMB with marked basic geometric parameters. In Table 1, there are listed parameters of the HMB.

The air gap δ between the stator and rotor in the real object is equal to 0.30 mm. In order to obtain good agreement between the simulation model and the real object,

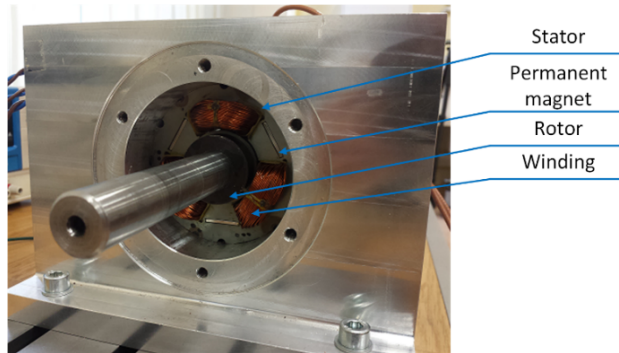


Fig. 1. The picture of the HMB

Table 1.

Parameters of the hybrid magnetic bearing

Parameter	Value
Stator outer diameter, d_{so}	86.0 mm
Stator inner diameter, d_{si}	70.0 mm
Rotor diameter, d_r	39.4 mm
Shaft diameter, d_s	20.0 mm
Nominal air gap, δ	0.3 mm
Leg width, w_l	12.0 mm
Bearing width, w_b	10.0 mm
Permanent magnet width, w_{pm}	20.0 mm
Permanent magnet height, h_{pm}	2.0 mm
Winding turns number, N	100
Maximal control current, $i_{x \max}, i_{y \max}$	2 A
Bias flux	76.1 mWb
Windings resistance, R_1, R_2, R_3	0.32 Ω
Mass of the rotor, m	1.54 kg
Eccentricity, e_s	11 μm

the value of the air gap in the calculation model has been increased to 0.39 mm. The reason for that is the manufacturing process, which creates a nonmagnetic layer in the real object [12]. Length of the nonmagnetic layer varies and takes values 0.04 mm or 0.05 mm as well as 0.07 mm [12, 13].

The magnetic force is generated by all poles due to the magnetic flux in the air gap of the ferromagnetic circuit. Nevertheless, only three poles with windings can control the value of the magnetic force along three coordinates s_1, s_2, s_3 (Fig. 2). The position of the HMB rotor is controlled by two controllers in the axis x and y

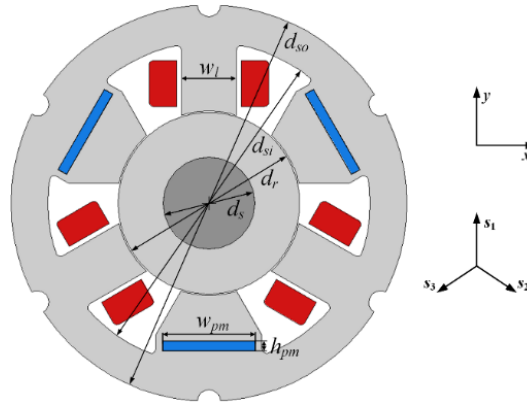


Fig. 2. Cross-section of the HMB

by adjusting control currents i_x and i_y . Currents excited in windings i_1, i_2, i_3 are calculated from the following expressions:

$$i_1 = i_y, \quad i_2 = -\frac{1}{2}i_y + \frac{\sqrt{3}}{2}i_x, \quad i_3 = -\frac{1}{2}i_y + \frac{\sqrt{3}}{2}i_x. \quad (1)$$

Similarly, the position of the rotor in coordinates s_1, s_2, s_3 can be calculated from the following equations:

$$s_1 = y, \quad s_2 = -\frac{1}{2}y + \frac{\sqrt{3}}{2}x, \quad s_3 = -\frac{1}{2}y + \frac{\sqrt{3}}{2}x. \quad (2)$$

3. A field-circuit model of the hybrid magnetic bearing

The field-circuit model of the HMB consists of two components. The first part constitutes a set of ordinary differential equations that describes electrical circuits and mechanics. These expressions were derived from the Euler-Lagrange formulation. The electrical circuits of the HMB is governed by the following equations:

$$u_1 = R_1 i_1 + L_{d1}(s_1, i_1) \frac{di_1}{dt} + e_{v1}(s_1, i_1) \frac{ds_1}{dt}, \quad (3a)$$

$$u_2 = R_2 i_2 + L_{d2}(s_2, i_2) \frac{di_2}{dt} + e_{v2}(s_2, i_2) \frac{ds_2}{dt}, \quad (3b)$$

$$u_3 = R_3 i_3 + L_{d3}(s_3, i_3) \frac{di_3}{dt} + e_{v3}(s_3, i_3) \frac{ds_3}{dt}, \quad (3c)$$

where u_1, u_2, u_3 denote supplying voltages, R_1, R_2, R_3 indicate the resistance of the windings, L_{d1}, L_{d2}, L_{d3} denote the dynamic inductances of the windings, e_{v1}, e_{v2}, e_{v3} indicate the velocity-induced voltages.

The mechanics of the HMB is governed by the following equations:

$$m \frac{d^2x}{dt^2} = F_x(x, i_x) + m\omega^2 e_s \cos(\omega t), \quad (4a)$$

$$m \frac{d^2y}{dt^2} = F_y(y, i_y) - mg + m\omega^2 e_s \sin(\omega t), \quad (4b)$$

where F_x , F_y denote magnetic forces in axes x and y , respectively. Symbol ω indicates the rotational speed, e_s denotes the eccentricity, m indicates the mass of the rotor, while g denotes the acceleration of gravity.

The second part of the simulation model is composed of parameters such as magnetic forces F_x , F_y , dynamic inductances L_{d1} , L_{d2} , L_{d3} and velocity-induced voltages e_{v1} , e_{v2} , e_{v3} . These parameters were calculated from the 3D FEM and were implemented in MATLAB/Simulink software as look-up tables. Fig. 3 depicts the FEM of the HMB prepared in Ansoft Maxwell 3D software.

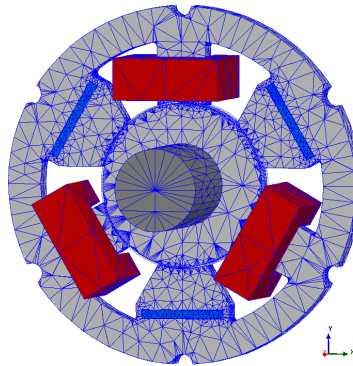


Fig. 3. The finite element model of the HMB

The FEM constitutes half of the real object geometry in order to reduce the number of tetrahedral elements. Adaptive meshing procedure was used in order to discretise calculation domains. The boundary of the simulation model was set on 40 mm from the stator and rotor, except for the symmetry plane that was set in the middle of the stator length. The zero Dirichlet boundary condition was assumed on the outer surface of the simulation model, while the zero Neumann boundary condition was assumed on the symmetry plane. The nonlinear characteristic of the magnetic material included in the FEM was tested with a closed magnetic circuit [14]. The magnetic field distribution was solved with the magnetostatic solver that has implemented the \vec{T} - Ω method. The magnetic field \vec{H} is represented by the magnetic scalar potential Ω and the current vector potential \vec{T} [15]:

$$\vec{H} = \vec{T} + \nabla\Omega, \quad (5)$$

where vector \vec{T} satisfies the equation:

$$\nabla \times \vec{T} = \vec{J}, \quad (6)$$

where \vec{J} is defined as current density.

In current-free regions, the magnetic field \vec{H} is calculated from the magnetic scalar potential Ω :

$$\vec{H} = \nabla \Omega. \quad (7)$$

Finite element analysis and principles of presented HMB function are given in [16]. Fig. 4 presents an example of the magnetic field distribution for the central position of the rotor ($y = 0$ mm) and the control current $i_y = 2$ A.

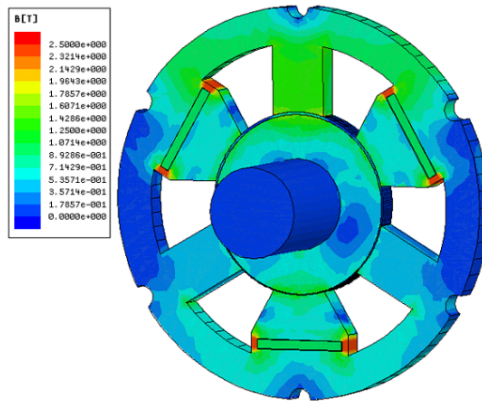


Fig. 4. The magnetic field distribution for the central position of the rotor ($y = 0$ mm) and the control current $i_y = 2$ A

The magnetic forces F_x , F_y (Fig. 5) were calculated from the virtual work method:

$$F_x(x, i_x) = \left. \frac{\partial W_{co}(x, i_x)}{\partial x} \right|_{i_x = \text{const}}, \quad (8a)$$

$$F_y(y, i_y) = \left. \frac{\partial W_{co}(y, i_y)}{\partial y} \right|_{i_y = \text{const}}, \quad (8b)$$

where W_{co} indicates the coenergy of the HMB.

Magnetic flux linkage ψ was obtained from the following equation:

$$\psi = N \iint_S \vec{B} \cdot d\vec{S}, \quad (9)$$

where N is the turn number of the stator windings and S denotes the area of the pole.

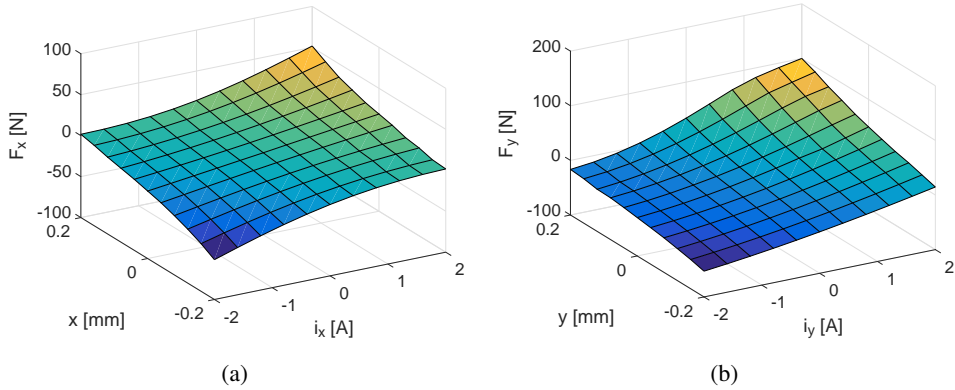


Fig. 5. The magnetic force F_x in relation to the position x and the control current i_x (a), the magnetic force F_y in relation to the position y and the control current i_y (b)

Magnetic flux linkages ψ_1 , ψ_2 , ψ_3 were employed to calculate the dynamic inductances and the velocity-induced voltages from the following expressions:

$$L_{d1}(s_1, i_1) = \frac{\partial \psi_1(s_1, i_1)}{\partial i_1}, \quad L_{d2}(s_2, i_2) = \frac{\partial \psi_2(s_2, i_2)}{\partial i_2}, \quad (10)$$

$$L_{d3}(s_3, i_3) = \frac{\partial \psi_3(s_3, i_3)}{\partial i_3}.$$

$$e_{v1}(s_1, i_1) = \frac{\partial \psi_1(s_1, i_1)}{\partial s_1}, \quad e_{v2}(s_2, i_2) = \frac{\partial \psi_2(s_2, i_2)}{\partial s_2}, \quad (11)$$

$$e_{v3}(s_3, i_3) = \frac{\partial \psi_3(s_3, i_3)}{\partial s_3}.$$

Fig. 6a presents the dynamic inductance L_{d1} in relation to the position s_1 and winding current i_1 , while Fig. 6b presents the velocity-induced voltage e_{v1} in relation to the position s_1 and winding current i_1 . Due to the HMB symmetry,

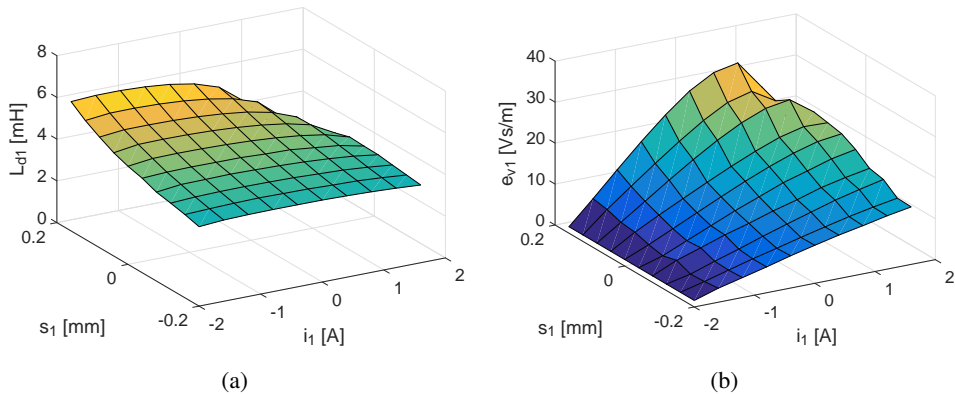


Fig. 6. The dynamic inductance L_{d1} in relation to the position p_1 and current i_1 (a), the velocity-induced voltage e_{v1} in relation to the position p_1 and current i_1 (b)

dynamic inductances L_{d2} , L_{d3} , as well as velocity-induced voltages e_{v2} , e_{v3} are identical to dynamic inductance L_{d1} and e_{v1} , respectively.

The current and displacement stiffness are important in the design process of the magnetic bearings control system [17]. In Table 2, there are listed parameters of the HMB that were calculated for central position of rotor ($x = 0$ mm, $y = 0$ mm) and lack of control currents ($i_x = 0$ A, $i_y = 0$ A).

Table 2.

Parameters of the HMB

Parameter	Value
Position stiffness, k_{sx}	122.57 N/mm
Current stiffness, k_{ix}	20.50 N/A
Position stiffness, k_{sy}	124.83 N/mm
Current stiffness, k_{iy}	20.60 N/A
Dynamic inductance, L_d	4.67 mH
Velocity-induced voltage, e_v	13.86 Vs/m

4. Implementation of the field-circuit model and closed loop control into MATLAB/Simulink software

The controller is critical to a magnetic bearing system because it allows levitation of the rotor and decides about its overall performance. The majority of control schemes have been investigated, like PD, PID, H_∞ , H_2 , LQR [18, 19, 21–23]. Among them, the most widely used is the PID controller, because of its simplicity. Position PID controllers are mostly used together with a current control scheme [24]. Fig. 7 presents the implementation of the FCM together with

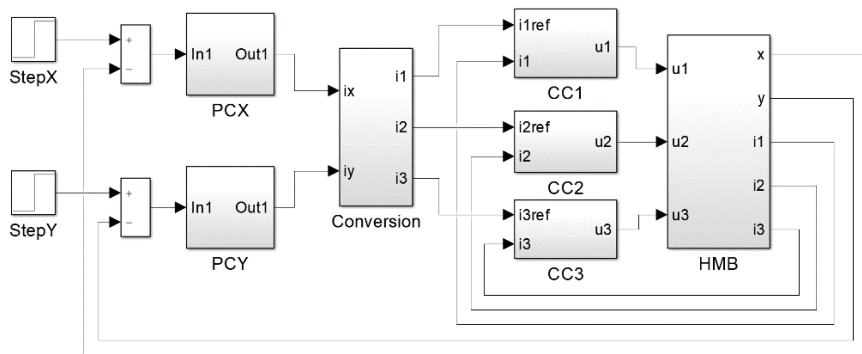


Fig. 7. Implementation of the control system in MATLAB/Simulink software (abbreviations: PCX – position controller in the axis x , PCY – position controller in the axis y , CC1 – current controller of the first winding, CC2 – current controller of the second winding, CC3 – current controller of the third winding)

the control system in MATLAB/Simulink software. The control system contains internal and external feedback loops. The internal loop is responsible for stabilization of the required current in windings of the HMB. It consists of three current controllers CC1, CC2, CC3, power amplifiers and electrical equations of the HMB. The external loop is responsible for stabilization of the rotor position. It is composed of two position controllers PCX, PCY, the conversion block of control currents to windings currents, underlying current control loops and mechanical equations of the HMB. The subsystem “HMB” constitutes the implementation of the FCM according to Eq. (1)–(4) and is presented in Fig. 8.

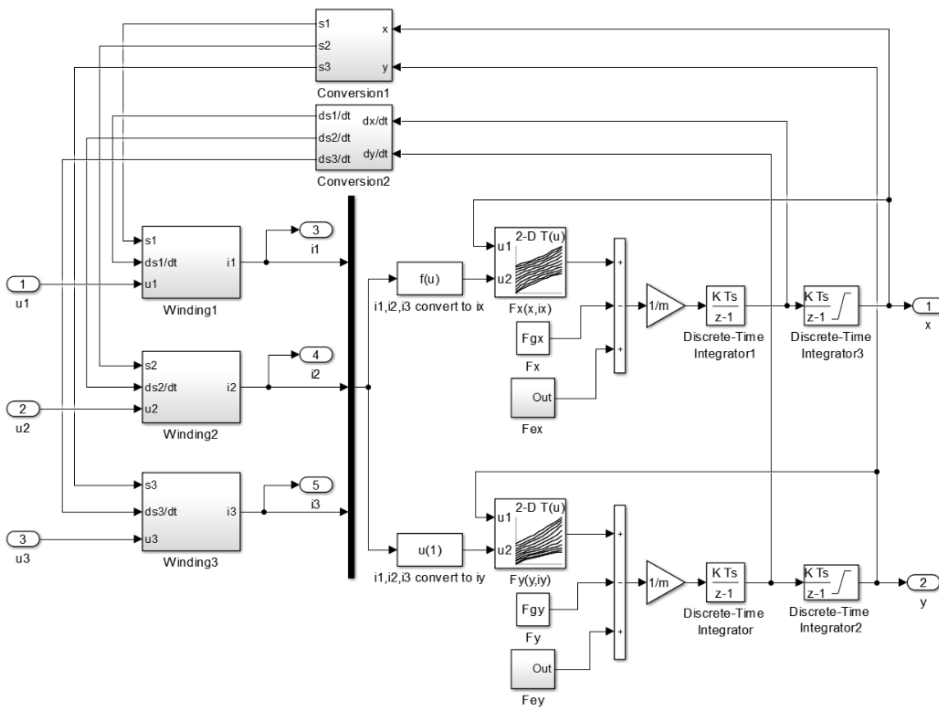


Fig. 8. The simulation model of the HMB

In Fig. 8, look-up tables $F_x(x, i_x)$ and $F_y(y, i_y)$ contain the previously calculated characteristics of the magnetic force in x and y axis. Subsystems “Winding1”, “Winding2” and “Winding3” constitute the implementation of the electrical equations (3) of the HMB. Fig. 9 depicts the implementation of Eq. (3a) that describes the first winding. Look-up tables $L_{d1}(s_1, i_1)$ and $e_{v1}(s_1, i_1)$ incorporate calculated characteristics of the dynamic inductance and the velocity-induced voltage.

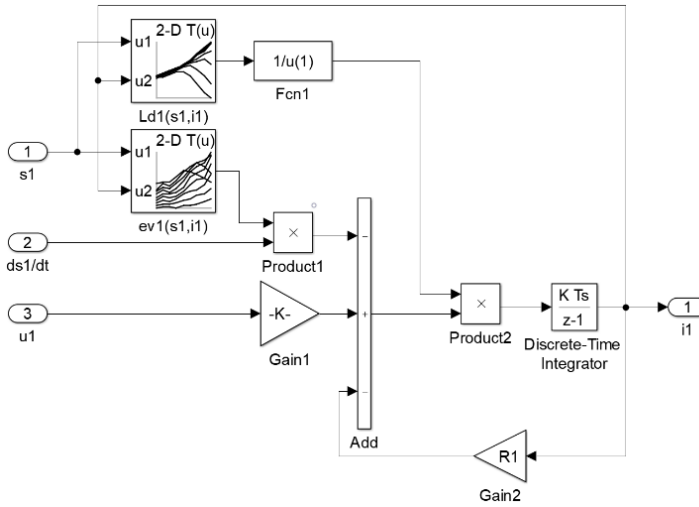


Fig. 9. The simulation model of the first winding

Parameters of the control system were derived from the linear model of the presented HMB described by the following equations:

$$m \frac{d^2 x}{dt^2} = k_{sx} x + k_{ix} i_x, \quad (12a)$$

$$m \frac{d^2 y}{dt^2} = k_{sy} y + k_{iy} i_y. \quad (12b)$$

The linearization point of the magnetic force results from the construction of the magnetic circuit and the shape of permanent magnets. For the presented HMB, the bias flux is equal to 76.1 mWb and magnetic field density in the poles with permanent magnets equals 0.634 T.

The positions of the rotor in axes x and y are controlled by two discrete PID controllers:

$$G_{PID}(z) = K_P + K_I \frac{T_s}{z-1} + K_D \frac{N}{1 + \frac{T_s N}{z-1}}, \quad (13)$$

where K_P , K_I and K_D are parameters of the controller. T_s denotes the sampling time and N indicates the filter coefficient of the derivative.

Windings currents i_1 , i_2 , i_3 are controlled by three discrete PI controllers:

$$G_{PI}(z) = K_P + K_I \frac{T_s}{z-1}. \quad (14)$$

All controllers contain an integrator anti-windup circuit [26]. Parameters of the controllers can be calculated from analytical expressions [24, 25]:

$$K_P = \frac{(p_1 p_2 + p_2 p_3 + p_1 p_3) m - k_s}{k_i}, \quad (15a)$$

$$K_I = \frac{-p_1 p_2 p_3 m}{k_i}, \quad (15b)$$

$$K_D = \frac{(-p_1 - p_2 - p_3) m}{k_i}, \quad (15c)$$

where: p_1, p_2, p_3 are required poles of the control system.

Complex poles p_1, p_2, p_3 decide about the dynamic response of the MB system and can be defined as follows:

$$p_1 = -\omega_n \xi + j \omega_n \sqrt{1 - \xi^2}, \quad (16a)$$

$$p_2 = -\omega_n \xi - j \omega_n \sqrt{1 - \xi^2}, \quad (16b)$$

where ω_n is the undamped natural frequency and ξ is the damping ratio.

The third pole p_3 should have a value that does not factor in the dynamic response of the MB system [24]. Different expressions on complex poles p_1 and p_2 that are derived from a comparison of the second order characteristic equation with the mass-spring-damper system are:

$$p_1 = -\frac{c}{2m} + j \sqrt{\frac{k}{m} - \frac{c^2}{4m^2}}, \quad (17a)$$

$$p_2 = -\frac{c}{2m} - j \sqrt{\frac{k}{m} - \frac{c^2}{4m^2}}, \quad (17b)$$

where c is the damping coefficient and k is the stiffness coefficient.

Value of the third complex pole p_3 should not factor in the dynamic response of the system and can be defined as follows:

$$p_3 = \sqrt{\frac{k}{m}}. \quad (18)$$

The stiffness coefficient k and damping coefficient c are common parameters that can be used to compare various types of bearing. Therefore, parameters of the PID controllers were calculated from equations (17a), (17b) and (18) for the stiffness coefficient k equal to 30000 N/m and the damping coefficient c equal to 100 Ns/m. Parameters of the PI current controllers were obtained by manual adjustment in order to obtain a fast response as well as acceptable overshooting. Values of the position controllers' coefficients are listed in Table 3, while Table 4 presents the values of the current controller coefficients.

Table 3.

Coefficient values of the position controllers

	K_P [A/m]	K_I [As/m]	K_D [A/ms]
Position controller in the axis x	8424	120 342	13.03
Position controller in the axis y	8852	126 500	15.26

Table 4.

Coefficient values of the current controllers

K_P [A/m]	K_I [As/m]
0.35	400

5. Simulation and measurement results

Fig. 10 presents an outline of a test bench for the HMB control system. The test bench consists of the HMB actuator, a computer with DS 1104 R&D controller board, switching power amplifiers, current transducers and proximity sensors. The values of currents are measured by three LEM LTS-6NP sensors. The distance between the stator and rotor is measured by two eddy current proximity sensors MDS10/MDT10. Their measurement range is from 0.5 mm to 2.5 mm and the frequency response 0÷10 kHz. The board DS1104 carries out the following tasks: analog to digital conversion of the current and position signals, execution of three PI current controllers and execution of two PID position controllers as well as generation of the PWM signals for switching power amplifiers. The controller board DS 1104 R&D has four 12-bit A/D converters and one 16-bit A/D converter. Additionally, the 16-bit A/D converter has installed the 4-channel analog multiplexer. All A/D converters use a successive approximation algorithm and internal sample-and-hold circuit to convert an analog signal to the digital value. The current signal is converted simultaneously by four 12-bit A/D converters with the frequency 20 kHz and the resolution 1.693 mA/bit. The position signals in the axis x and y are converted one after another by the 16-bit A/D converter with frequency 10 kHz and the resolution 0.03815 $\mu\text{m/bit}$. The delay between two samples of the

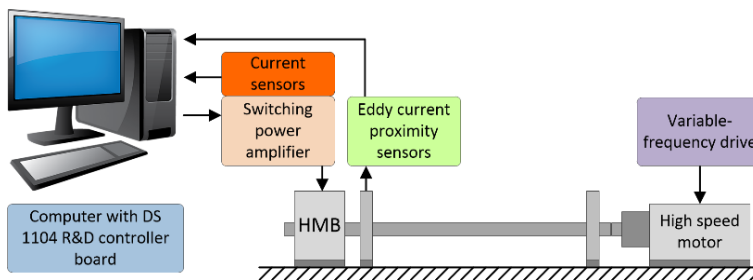


Fig. 10. An outline of a test bench for the HMB control system

rotor position shouldn't be greater than $2 \mu\text{s}$. The switching power amplifiers work with frequency of 50 kHz.

Verification of the FCM was done by comparison of time responses obtained from the simulation model and the real object. Three dynamic states were considered: step change $\pm 20 \mu\text{m}$ in the x -axis, step change $\pm 20 \mu\text{m}$ in the y -axis and the rotor rotation with the frequency of 100 Hz. Fig. 11 presents time responses of control currents i_x and i_y as well as the rotor position in the axis x and y for the step change $\pm 20 \mu\text{m}$ of the rotor position along the x -axis.

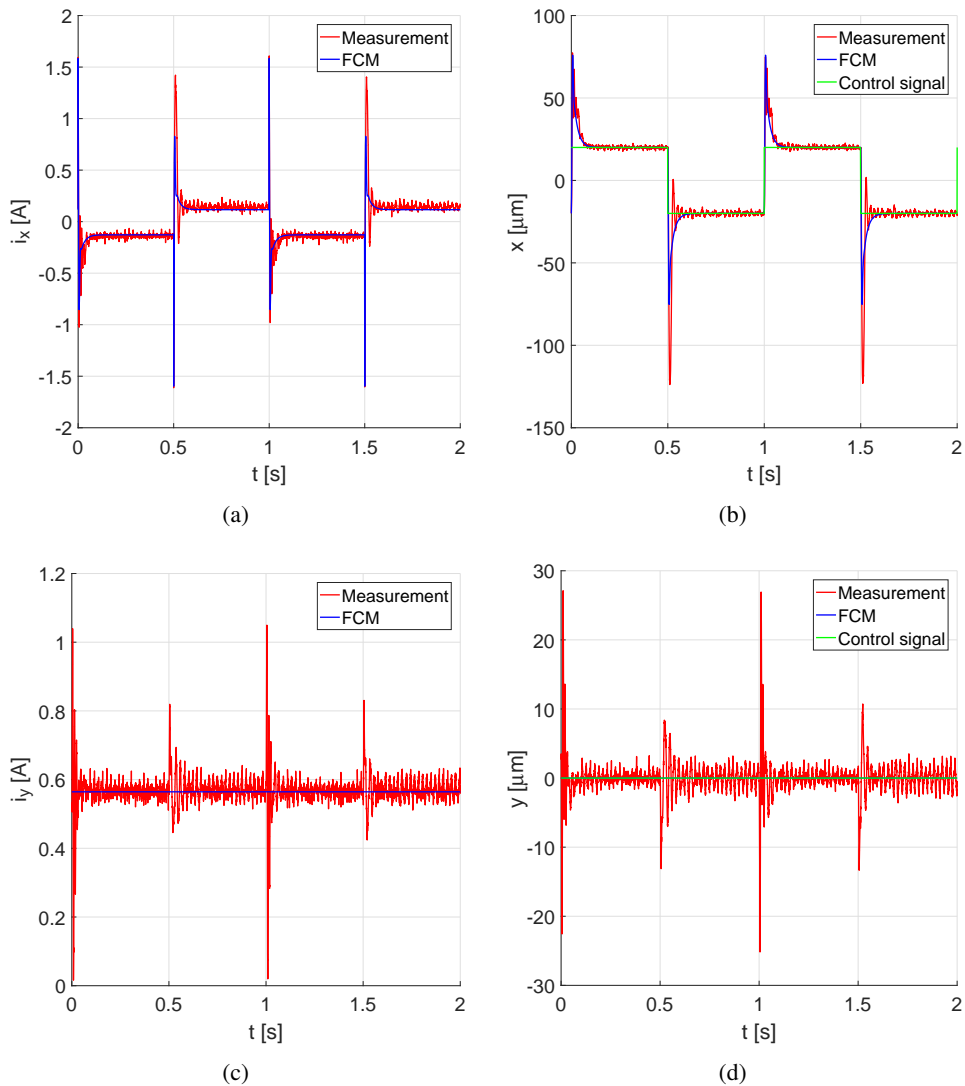


Fig. 11. Time responses of the control current i_x (a), the rotor position x (b), the control current i_y (c) and the rotor position y (d) for the step change $\pm 20 \mu\text{m}$ of the rotor position along the x -axis

A noticeable interference signal appearing in the measurements is caused by switching power amplifiers and insufficient electromagnetic shielding of the analog signals. Similar noisy signals can be found in various papers [19, 20]. Albeit, in the real object clearly one can see disruption of the rotor position in the axis orthogonal to the axis with the step change of the rotor position (Fig. 11b at 0.0 s, 0.5 s, 1.0 s etc.). That behaviour indicates the cross-coupling between both axes and is responsible for significant change of the control current in the orthogonal axis.

Fig. 12 presents time responses of the control currents i_x and i_y as well as the rotor position in the axis x and y for the step change $\pm 20 \mu\text{m}$ of the rotor position along the y -axis.

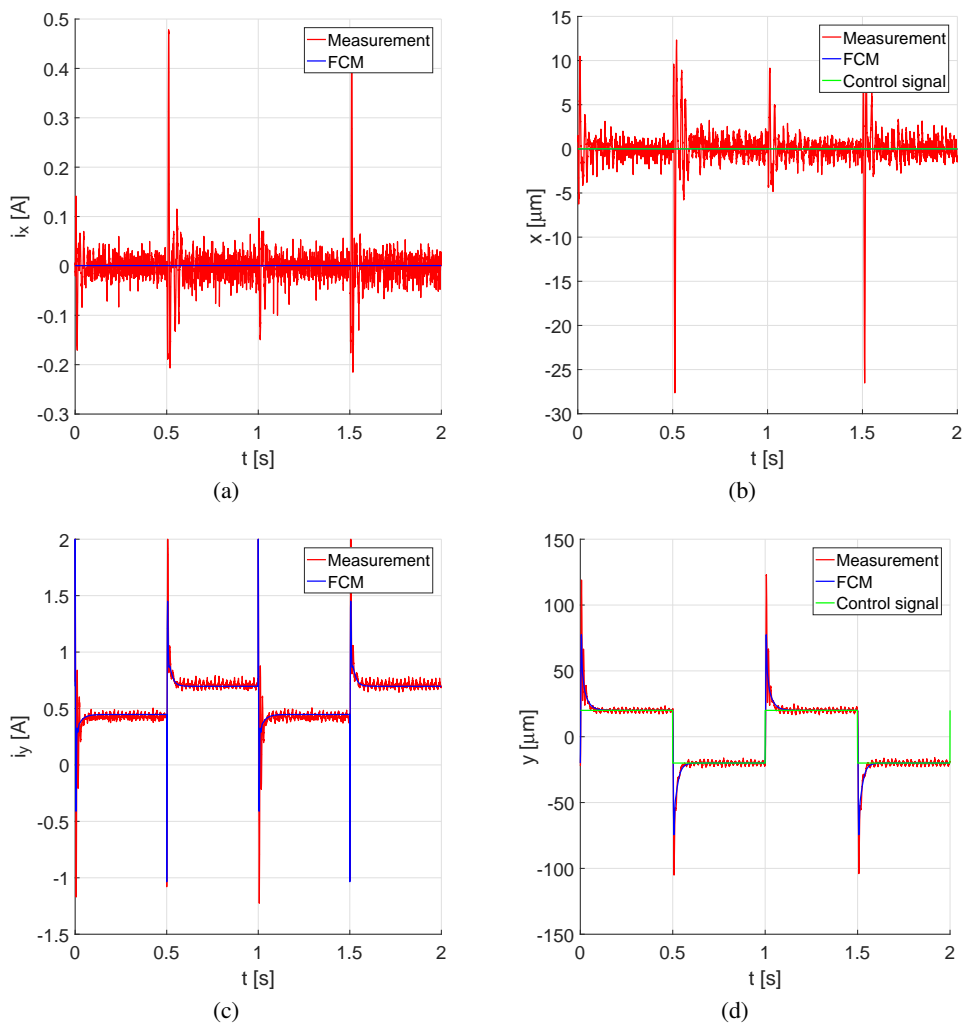


Fig. 12. Time responses of the control current i_x (a), the rotor position x (b), the control current i_y (c) and the rotor position y (d) for the step change $\pm 20 \mu\text{m}$ of the rotor position along the y -axis

The accuracy of the FCM is assessed by calculations of root mean squared errors (RMSEs) between the measurement and simulation. The RMSEs were calculated from the following expressions:

$$RMSE_x = \sqrt{\frac{1}{n} \sum_{k=1}^n (x_{\text{measurement}}(k) - x_{\text{simulation}}(k))^2}, \quad (19a)$$

$$RMSE_{i_x} = \sqrt{\frac{1}{n} \sum_{k=1}^n (i_{x\text{-measurement}}(k) - i_{x\text{-simulation}}(k))^2}, \quad (19b)$$

$$RMSE_y = \sqrt{\frac{1}{n} \sum_{k=1}^n (y_{\text{measurement}}(k) - y_{\text{simulation}}(k))^2}, \quad (19c)$$

$$RMSE_{i_y} = \sqrt{\frac{1}{n} \sum_{k=1}^n (i_{y\text{-measurement}}(k) - i_{y\text{-simulation}}(k))^2}. \quad (19d)$$

where n denotes the number of measurement points.

In Tab. 5, there are listed values of the RMSEs calculated for transient responses presented in Fig. 11 and 12. It can be noticed that smaller values of errors appear in the y -axis.

Table 5.

The RMSE values for transient responses

	A step change of the rotor position in the x -axis	A step change of the rotor position in the y -axis
$RMSE_x$	7.512 μm	2.378 μm
$RMSE_{i_x}$	111.2 mA	40.01 mA
$RMSE_y$	2.726 μm	4.081 μm
$RMSE_{i_y}$	50.72 mA	82.79 mA

Fig. 13a and 13b present time responses of the control currents i_x and i_y for the rotor rotation with the frequency of 100 Hz.

Fig. 14 depicts the position of the rotor in x and y axis for the rotor rotation with the frequency of 100 Hz. It can be seen that the trajectory of the rotor movement obtained from the FCM as well as from measurement is not a circle. The reason for this is the asymmetrical characteristic of the magnetic force in the y -axis (Fig. 5b). Irregular rotation of the rotor and oscillations in control currents are caused by the mechanical and electrical run-out [27].

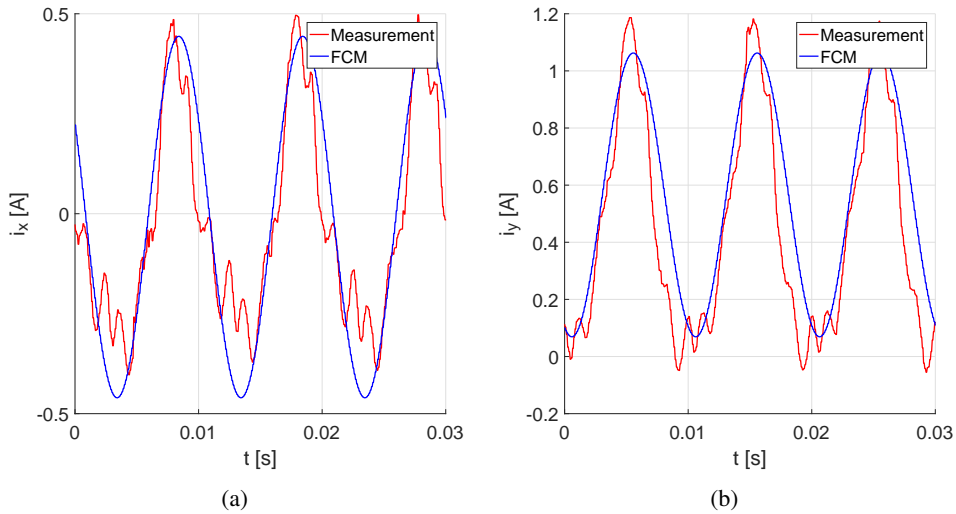


Fig. 13. Time responses of the control currents i_x (a) and i_y (b) for the rotor rotation with the frequency of 100 Hz

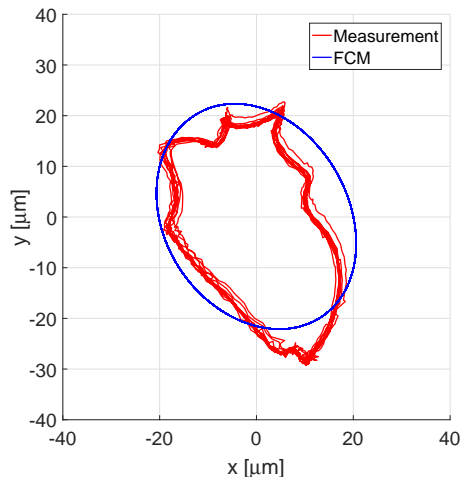


Fig. 14. The rotor position in x and y axes for the rotor rotation with the frequency of 100 Hz

6. Conclusions

The field-circuit model of the hybrid magnetic bearing dedicated to simulation of the transient state is presented in the paper. The described model couples an electromagnetic 3D finite element model with equations of electrical circuits and mechanics. The 3D finite element model encompasses the nonlinear characteristic of the magnetic material and the complicated shape of the HMB magnetic circuit

with permanent magnets. The results of the magnetic field calculation are incorporated into the simulation model as look-up tables. The advantages of the proposed field-circuit method are low computation effort and short calculation time, which is due to the fact that electromagnetic parameters of the HMB are calculated once. The simulation model includes controllers required for the magnetic bearing levitation, as well. The simulation model was verified by comparison of control currents and the rotor position with the real object. Satisfactory concordance between the simulation model and the real object for testing various control schemes was achieved.

Manuscript received by Editorial Board, October 15, 2018;
final version, April 14, 2019.

References

- [1] G. Schweitzer and H. Maslen. *Magnetic bearings, theory, design, and application to rotating machinery*. Springer, 2009.
- [2] L. Ji, L. Xu, and Ch. Jin. Research on a low power consumption six-pole heteropolar hybrid magnetic bearing. *IEEE Transactions on Magnetics*, 49(8):4918–4926, 2013. doi: [10.1109/TMAG.2013.2238678](https://doi.org/10.1109/TMAG.2013.2238678).
- [3] A. Piłat. Active magnetic suspension and bearing. In G. Petrone and G. Cammarata, *Recent advances in modelling and simulation*, chapter 24, pages 453–470. I-Tech Education and Publishing, 2008.
- [4] A. Iordanidis, R. Wrobel, D. Holliday, and P. Mellor. A field-circuit model of an electrical gearbox actuator. In *Proceedings of Second International Conference on Power Electronics, Machines and Drives (PEMD 2004)*, pages 21–26, Edinburgh, UK, 31 March–2 April, 2004. doi: [10.1049/cp:20040410](https://doi.org/10.1049/cp:20040410).
- [5] B. Tomczuk, A. Waindok, and D. Wajnert. Transients in the electromagnetic actuator with the controlled supplier. *Journal of Vibroengineering*, 14(1):39–44, 2012. <https://www.jvejournal.com/article/10546/pdf>.
- [6] B. Tomczuk and M. Sobol. A field-network model of a linear oscillating motor and its dynamics characteristics. *IEEE Transactions on Magnetics*, 41(8):2362–2367, 2005. doi: [10.1109/TMAG.2005.852941](https://doi.org/10.1109/TMAG.2005.852941).
- [7] B. Tomczuk and D. Wajnert. Field-circuit model of the radial active magnetic bearing system. *Electrical Engineering*, 100(4):2319–2328, 2018. doi: [10.1007/s00202-018-0707-7](https://doi.org/10.1007/s00202-018-0707-7).
- [8] J. Zimon, B. Tomczuk, and D. Wajnert. Field-circuit modeling of AMB system for various speeds of the rotor. *Journal of Vibroengineering*, 14(1):165–170, 2012. <https://www.jvejournal.com/article/10565/pdf>.
- [9] M. Łukaniszyn, M. Jagieła and, R. Wróbel. Electromechanical properties of a disc-type salient pole brushless DC motor with different pole numbers. *COMPEL: The International Journal for Computation and Mathematics in Electrical and Electronic Engineering*, 22(2):285–303, 2003. doi: [10.1108/03321640310459216](https://doi.org/10.1108/03321640310459216).
- [10] M. Łukaniszyn, R. Wróbel, and M. Jagieła. Field-circuit analysis of construction modifications of a torus-type PMDC motor. *COMPEL: The International Journal for Computation and Mathematics in Electrical and Electronic Engineering*, 22(2):337–355, 2003. doi: [10.1108/03321640310459261](https://doi.org/10.1108/03321640310459261).

- [11] R. Pollanen, J. Nerg, and O. Pyrhonen. Reluctance network method based dynamic model of radial active magnetic bearings. In *Proceedings of the 2005 IEEE International Magnetics Conference (INTERMAG)*, pages 715–716, Nagoya, Japan, 4–8 April, 2005. doi: [10.1109/INTMAG.2005.1464144](https://doi.org/10.1109/INTMAG.2005.1464144).
- [12] M. Antila, E. Lantto and A. Arkkio. Determination of forces and linearized parameters of radial active magnetic bearings by finite element technique. *IEEE Transactions on Magnetics*, 34(3):684–694, 1998. doi: [10.1109/20.668066](https://doi.org/10.1109/20.668066).
- [13] B. Polajzer, G. Stumberger, J. Ritonja, and D. Dolinar. Variations of active magnetic bearings linearized model parameters analyzed by finite element computation. *IEEE Transactions on Magnetics*, 44(6):1534–1537, 2008. doi: [10.1109/TMAG.2007.916650](https://doi.org/10.1109/TMAG.2007.916650).
- [14] B. Tomczuk and D. Koterias. 3D Field Analysis in 3-phase amorphous modular transformer under increased frequency operation. *Archives of Electrical Engineering*, 64(1):119–127, 2015. doi: [10.1515/ae-2015-0011](https://doi.org/10.1515/ae-2015-0011).
- [15] Z. Badics and Z.J. Cendes. Source field modeling by mesh incidence matrices. *IEEE Transactions on Magnetics*, 43(4):1241–1244, 2007. doi: [10.1109/TMAG.2006.890967](https://doi.org/10.1109/TMAG.2006.890967).
- [16] D. Wajnert and B. Tomczuk. Simulation for the determination of the hybrid magnetic bearing’s electromagnetic parameters. *Przegląd Elektrotechniczny*, 93(2):157–160, 2017. <http://pe.org.pl/articles/2017/2/34.pdf>.
- [17] A. Mystkowski. Energy saving robust control of active magnetic bearings in flywheel. *Acta Mechanica et Automatica*, 6(3):72–76, 2012. http://www.actawm.pb.edu.pl/volume/vol6no3/MYSTKOWSKI_EN_2012_017.pdf.
- [18] A. Piłat. PD control strategy for 3 coils AMB. In *Proceedings of the 10th International Symposium on Magnetic Bearing*, pages 34–39, Martigny, Switzerland, August 21–23, 2006.
- [19] D. Kozanecka. *Digitally controlled magnetic bearing*. Łódź University of Technology, 2001 (in Polish).
- [20] S. Myburgh, G. von Schoor, and E. O. Ranft. A non-linear simulation model of an active magnetic bearings supported rotor system. In *Proceedings of The XIX International Conference on Electrical Machines (ICEM 2010)*, pages 1–6, Rome, Italy, 6–8 September 2010. doi: [10.1109/ICELMACH.2010.5607982](https://doi.org/10.1109/ICELMACH.2010.5607982).
- [21] Z. Gosiewski and A. Mystkowski. Robust control of active magnetic suspension: Analytical and experimental results. *Mechanical Systems and Signal Processing*, 22(6):1297–1303, 2008. doi: [10.1016/j.ymsp.2007.08.005](https://doi.org/10.1016/j.ymsp.2007.08.005).
- [22] A. Mystkowski. *Robust control of vibration of the magnetically suspended rotor*. Ph.D. Thesis, AGH University of Science and Technology, Cracow, Poland, 2007 (in Polish).
- [23] A. Piłat. *Control of magnetic levitation systems*. Ph.D. Thesis, AGH University of Science and Technology, Cracow, Poland, 2002 (in Polish).
- [24] Z. Gosiewski. *Magnetic bearings for rotating machines. Controlling and research*. Biblioteka Naukowa Instytutu Lotnictwa, 1999 (in Polish).
- [25] K. Falkowski. *The development of the laboratory model of the gyroscope with the magnetically levitating rotor and its research*. Ph.D. Thesis, Warsaw University of Technology, Warsaw, Poland, 1999 (in Polish).
- [26] G.F. Franklin, J.D. Powell and A. Emami-Naeini. *Feedback control of dynamic systems*, Prentice Hall, 2002.
- [27] S. Szymaniec. “Measurement paths” used to measure relative vibrations in electric machines. *Zeszyty Problemowe – Maszyny Elektryczne*, 81:55–60, 2009 (in Polish).